https://doi.org/10.1007/s41230-023-3037-y

Effect of slow shot speed on externally solidified crystal, porosity and tensile property in a newly developed high-pressure die-cast Al-Si alloy

Wen-ning Liu[1], Wei Zhang[3], Peng-yue Wang[4], Yi-xian Liu[1], Xiang-yi Jiao[1], Ao-xiang Wan[1], Cheng-gang Wang[4], Guo-dong Tong[3], and *Shou-mei Xiong[1, 2]

1. School of Materials Science and Engineering, Tsinghua University, Beijing 100084, China

2. Key Laboratory for Advanced Materials Processing Technology, Tsinghua University, Beijing 100084, Beijing

3. China FAW Group Co., Ltd., Changchun 130013, China

4. China FAW Foundry Co., Ltd., Changchun 130013, China

Abstract: The effect of slow shot speed on externally solidified crystal (ESC), porosity and tensile property in a newly developed high-pressure die-cast Al-Si alloy was investigated by optical microscopy (OM), scanning electron microscopy (SEM) and laboratory computed tomography (CT). Results showed that the newly developed AlSi9MnMoV alloy exhibited improved mechanical properties when compared to the AlSi10MnMg alloy. The AlSi9MnMoV alloy, which was designed with trace multicomponent additions, displays a notable grain refining effect in comparison to the AlSi10MnMg alloy. Refining elements Ti, Zr, V, Nb, B promote heterogeneous nucleation and reduce the grain size of primary α-Al. At a lower slow shot speed, the large ESCs are easier to form and gather, developing into the dendrite net and net-shrinkage. With an increase in slow shot speed, the size and number of ESCs and porosities significantly reduce. In addition, the distribution of ESCs is more dispersed and the net-shrinkage disappears. The tensile property is greatly improved by adopting a higher slow shot speed. The ultimate tensile strength is enhanced from 260.31 MPa to 290.31 MPa (increased by 11.52%), and the elongation is enhanced from 3.72% to 6.34% (increased by 70.52%).

Keywords: hypoeutectic Al-Si alloy; high pressure die casting; porosity; externally solidified crystal; tensile property

CLC numbers: TG146.21 **Document code:** A **Article ID:** 1672-6421(2024)01-011-09

1 Introduction

As more attention is being directed towards energy conservation and environmental protection, lightweight design has become a prominent trend in automobile development [1-3]. Hypoeutectic Al-Si alloy is widely used in the aerospace and automobile industry for its small specific gravity, high specific strength, good casting performance and excellent processing performance [4-5]. However, when pursuing lightweight construction, hypoeutectic Al-Si alloys are subjected to higher mechanical property requirements. To meet the demands for improved ultimate tensile properties and elongation, it becomes necessary to develop new Al-Si alloys.

High pressure die casting (HPDC), as a final shape or near-final shape material processing method, has the advantages of good product quality, high production efficiency and high dimensional accuracy of castings [6-7]. However, due to the rapid cooling rate during die casting, some crystals nucleate and grow up mostly in a dendritic form named externally solidified crystals (ESCs) [7-8]. Simultaneously, the air exists in the upper part of the cavity will not be filled with the melt. As the plunger moves forward, a mixture of ESCs, air, and melt is injected into the die cavity [9]. This unique solidification process of HPDC often leads to the formation of a heterogeneous structure, characterized by defects such as defect bands and porosity. Laukli et al. [10] studied the solidification characteristics related to the HPDC process and the alloy composition which influenced the formation of grain and defect, and the results showed that the alloy composition and the process parameters play an important role in the formation of ESCs and defects. In another study, Dou et al. [11] used computer-aided engineering (CAE) to simulate the entire HPDC process. They successfully

***Shou-mei Xiong**

Male, Ph.D., Professor. Research interests: Al and Mg alloy high pressure die casting and microstructure simulation during solidification.

E-mail: smxiong@tsinghua.edu.cn
Received: 2023-03-15; Accepted: 2023-07-27

predicted the formation of entrained air and oxides indicator, and established a correlation between operational parameters, casting defects, and mechanical properties.

The microstructure and mechanical properties of die castings have a great relationship with process parameters. Wang et al. [12] studied the microstructure and mechanical properties of high-pressure die-cast AZ91D magnesium alloy under different slow shot speeds. Results showed that slow shot speed played an important role in the porosity formation. A lower slow shot speed can reduce the formation of porosity in vacuum die casting. Tsoukalas et al. [13] studied the effect of die casting parameters on porosity. They found that all of the considered parameters and parameter interactions had an influence on the porosity formation, particularly the intensification pressure, plunger second velocity, and die cavity filling time. The predicted range of casting porosity under the optimal die casting parameters was $1.53\%<\hat{\mu}<1.64\%$. Fu et al. [14] studied the low-pressure die casting of AM50 magnesium alloy under different process parameters. They found that the grains became coarser and the mechanical properties including yield strength, ultimate tensile strength, and elongation became worsen with the increasing filling time. Cao et al. [15] investigated the influence of process parameters on the microstructural features. It was found that a higher injection speed could result in more broken dendrites and spherical grains. Jiao et al. [16] studied the influence of the slow shot speed on porosity of high-pressure die-cast AlSi17Cu2.5 alloy, and found that various slow shot speeds could lead to a significant influence on the distribution of porosity.

Some research results show the externally solidified crystals (ESCs) have a certain contribution to porosity formation. Tzamtzis et al. [17] studied the microstructure of ESCs in die-cast AZ91D alloy. Results showed a higher area fraction of ESCs promoted the porosity formation. Kim et al. [18] found that process parameters influenced the area fraction of ESCs. The content of ESCs showed a positive proportional relationship with porosity. In our previous work, Li et al. [19] studied the porosity induced by ESCs in high pressure die casting AM60 alloy. It was found that there were two kinds of porosities induced by ESCs. The first one was small in size, spherical in geometry, and distributes in the center of microstructure. The other one was relatively larger in size, which had an interconnected structure. But, the influence of process parameters on porosity was not considered. Jiao et al. [20] studied the effect of ESCs on the porosity and mechanical properties of die casting AlSi10MnMg alloy. With the decrease of fast shot speed and slow shot speed, the ESCs were found to be coarsen from a fine globular shape into a large dendritic shape, and the area fraction was reduced. According to the linear fitting results, there was a quantitative link between ESCs' strength and elongation. However, few studies focused on the relationship among ESCs, porosity and tensile properties.

In this study, the microstructure and mechanical properties of a newly developed hypoeutectic AlSi9MnMoV alloy were investigated. Furthermore, special attention was given to examining the relationship among ESCs, porosity, and tensile properties under varying slow shot speeds.

2 Experimental procedure

The composition of the newly developed hypoeutectic AlSi9MnMoV alloy is listed in Table 1. Figure 1(a) shows the die casting samples including three bars and one plate produced by a TOYO BD-350V5 cold chamber die casting machine. The standard tensile bar is shown in Fig. 1(b). The central section of the tensile bar, measuring Φ6.4 mm×10 mm, was subjected to laboratory computed tomography (CT) scanning to detect and analyze any existing pores under different slow shot speeds. The operation voltage and current were set as 110 kV and 100 µA, respectively. Two-dimensional slices were collected and subsequently reconstructed into a three-dimensional shape using Avizo software. Additionally, the cross section of the tensile bar was prepared for optical micrography (OM) and scanning electron microscopy (SEM) analysis. Figure 1(c) shows the processing parameters adopted during the high pressure die casting. The casting pressure was 87 MPa. Two different slow shot speeds of 0.1 $m \cdot s^{-1}$ and 0.4 $m \cdot s^{-1}$ were used. At the mean time, the AlSi10MnMg alloy was used for comparative study, and the experimental conditions were kept all the same as those of the Al9SiMnMoV alloy.

Table 1: Chemical composition of a newly developed hypoeutectic Al9SiMnMoV alloy (wt.%)

Si	Fe	Mo	Mn	V	Zr	B	Ti	Nb	Ni	Sr	Al
9	0.4	0.5	0.3	0.4	0.25	0.2	0.1	0.1	0.1	0.07	Bal.

The SiC sandpapers of #400, #800, #1200, #1500 and #2000 were used to prepare metallography samples. Then, diamond paste was used to prepare a bright and seamless surface. The corrosive solution, known as Murakami reagent, was prepared by combining 10 g of NaOH, 5 g of $K_3(Fe(CN))_6$, and 60 mL of H_2O. This solution was utilized to create corrosion patterns. The tensile mechanical property was tested using an MTS E45 stretching machine with a loading rate of 2 $mm \cdot min^{-1}$. A software named Avizo was used to identify the ESCs in samples. The primary α-Al can be extracted by the different contrast. Both ESCs and $(\alpha\text{-Al})_{II}$ are primary α-Al, while ESCs nucleated in the shot sleeve and $(\alpha\text{-Al})_{II}$ nucleated in the die cavity [20]. The ESCs and $(\alpha\text{-Al})_{II}$ were distinguished by the size difference. The average diameter (D) of the primary α-Al can be estimated by:

$$D = 2\sqrt{\frac{A}{\pi}} \tag{1}$$

where A means the real area of ESCs. The primary α-Al with an average diameter (D) exceeding 10 µm could be considered as ESCs [20].

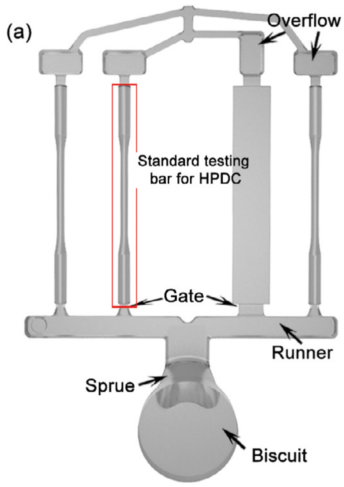

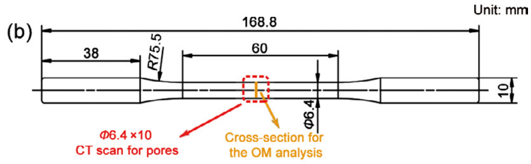

(c)

Processing parameters adopted during casting
Melting temperature (°C): 695
Initial mold temperature (°C): 150
Slow shot speed (m·s^{-1}): 0.1, 0.4
Fast shot speed (m·s^{-1}): 2.75
Mold holding time (s): 8
Cooling material: H13 mold steel with water tube

Fig. 1: Configuration of die casting samples by HPDC (a), standard bar for tensile testing (b), and processing parameters adopted during die casting (c)

3 Results and discussion

3.1 Microstructure of die casting AlSi9MnMoV alloy

Figures 2(a) and (b) show the SEM results of the AlSi9MnMoV alloy by high pressure die casting under a slow shot speed of 0.1 m·s^{-1}. The microstructure consists of coarse ESCs, fine (α-Al)$_{II}$, eutectic Si and iron-rich phase. The average size of ESCs is about 30 µm, and the average size of (α-Al)$_{II}$ is about 5 µm. The eutectic Si presents a fibrous shape, and iron-rich phase is mainly distributed around the eutectics. Figures 2(c–c5) indicate the elements Fe, Mn, Mo and V are mainly distributed in the iron-rich phase. Iron (Fe) is the essential element in die casting alloy because of the demolding requirement. High content of Fe promotes casting demolding and protects die-casting mold. However, Fe has a low solubility in Al, and promotes the formation of iron-rich phase. The presence of coarse Chinese-like and plate-like iron-rich phases can lead to a significant decrease in mechanical properties [20]. In the AlSi9MnMoV alloy, the iron-rich phase observed is predominantly bulk-like with a relatively small size range of 1–5 µm. The addition of Mn, Mo, V elements changes the morphology and reduces the size of iron-rich phases, suggesting a good refining and modifying effect.

Figures 2(d) and (e) show the EBSD results of AlSi9MnMoV alloy and AlSi10MnMg alloy from surface to center under the same process parameters of slow shot speed 0.1 m·s^{-1} and fast shot speed 2.75 m·s^{-1}. The melting temperature of both the alloys was 695 °C. The AlSi9MnMoV alloy designed by trace multicomponent presents a significant refinement effect compared with AlSi10MnMg alloy. The presence of Ti [21], Zr [22], V [23], Nb [24], B [25] in AlSi9MnMoV melt promotes the formation of metallic compounds, including Al_3Ti, Al_3V, Al_3Zr, Al_3Nb, TiB_2, NbB_2. These compounds serve as effective heterogeneous nucleation sites for primary α-Al during solidification due to their low lattice mismatch with the Al matrix. The increased number of nuclei contributed to the refinement of primary α-Al grains. The grain size of AlSi9MnMoV alloy was measured to be around 19 µm, whereas the grain size of the AlSi10MnMg alloy was approximately 67 µm. These results indicate that the newly developed alloy, AlSi9MnMoV, exhibits superior grain refining performance compared to the AlSi10MnMg alloy.

3.2 Microstructure of AlSi9MnMoV alloy under different slow shot speeds

Figures 3(a) and (b) show the optical micrograph of the AlSi9MnMoV alloy under different slow shot speeds (V_L). A typical die casting heterogeneous microstructure is observed with the chilling fine grains in the skin layer, the silicon-rich zone in the defect band, and the ESCs-rich zone in the center. The grain size of skin layer is small due to the intensive heat transfer from the casting to mold. The position of defect band is marked by red dotted lines. The defect band is caused by shear stress and solute redistribution under intensification pressure. The shear stress exerted by the melt flow under intensification pressure on the partially solidified alloy causes grain rotation, leading to an expansion of the semi-solid region and facilitating feeding of the remaining melt into this region [26-28]. During the solidification process, as the remaining melt approaches the eutectic point, a defect band is formed. With the increase of slow shot speed, this defect band moves closer to the center. The defect band is located at distances of 879 µm and 1,058 µm from the surface when the shot speed is between 0.1 m·s^{-1} and 0.4 m·s^{-1}, respectively. When ESCs nucleate in the shot sleeve, they experience a centripetal force towards the center due to the shear stress exerted by the high-speed liquid metal. Then, the ESCs gather together and form a α-Al rich region. Figures 3(c) and (d) show the optical micrograph along the radial direction at slow shot speeds of 0.1 m·s^{-1} and 0.4 m·s^{-1}, respectively. The surface region belongs to the skin layer, characterized by a fine grain size resulting from rapid cooling. Moving towards the middle, the position of the defect band exhibits a higher content of eutectics. It is found that coarse ESCs and pores exist in the center. The developed dendrites

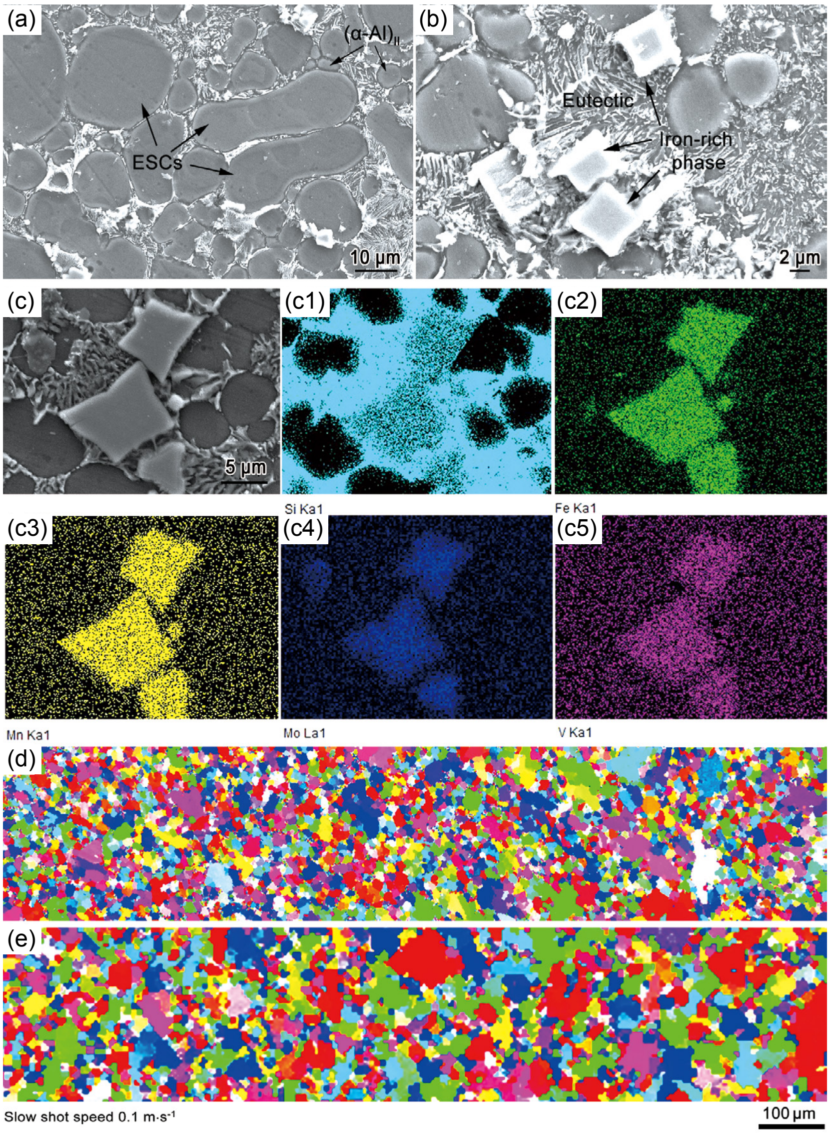

Fig. 2: SEM results of ESCs and (α-Al)$_{II}$ (a), eutectic and Fe-rich phase (b), map scanning (c), EBSD results of AlSi9MnMoV alloy (d), and AlSi10MnMg alloy (e)

form the dendrite net, causing the metal liquid is blocked. Unfilled spaces between dendrites can result in shrinkages. Moreover, at slower shot speeds, air is more likely to be entrapped, leading to pore formation. With the slow shot speed increases, the ESCs are refined and the number of pores and shrinkages is reduced.

Figure 4(a) shows the SEM-detected areas of the sample, including surface (c), middle (d) and center (e). Figure 4(b) shows the EPMA line scanning results of Al, Si, Fe, Mn and Mo elements from surface to center. Fe and Mn elements exhibit high levels in certain areas and keep a quite consistency. The distribution of Mo element is almost consistent, but the content is low. The Fe and Mn elements are mainly distributed in the middle and center while the Mo element is enriched in the middle. Figures 4(c–e) show the SEM map scanning results of surface, middle (defect band) and center. From Fig. 4(c1) to Fig. 4(e1), it can be seen Al elements mainly enrich in the center, which is agreed with the metallograph results. Correspondingly, Si is mainly distributed in the defect band compared with the surface and center [see in Figs. 4(c2, d2, e2)]. Fe and Mn

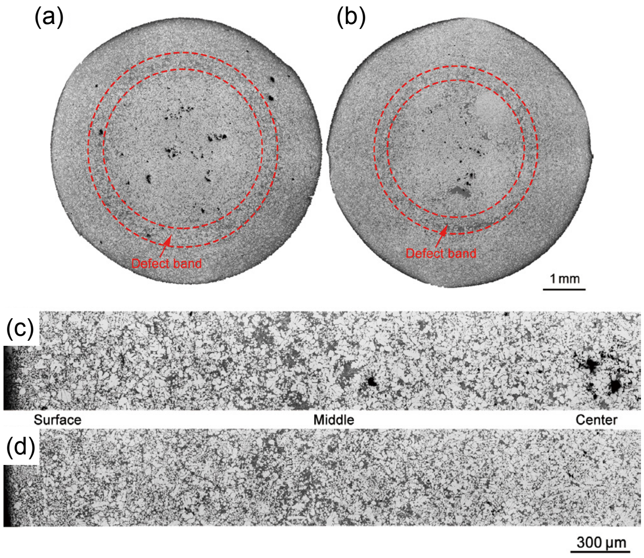

Fig. 3: Optical micrograph of cross section rod sample at V_L=0.1 m·s^{-1} (a), and V_L=0.4 m·s^{-1} (b); and optical micrograph along the radius at V_L=0.1 m·s^{-1} (c), and V_L=0.4 m·s^{-1} (d)

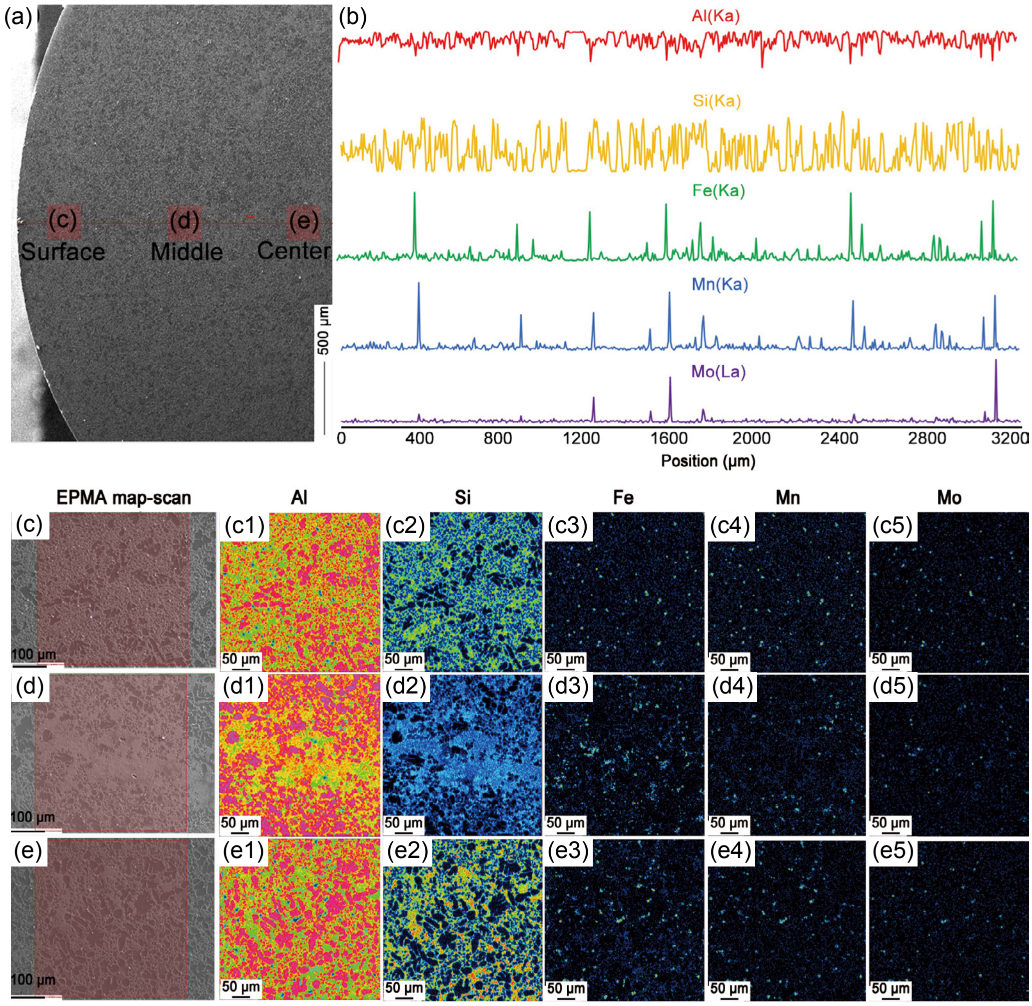

Fig. 4: SEM result of the cross section (a); EPMA line scanning results of Al, Si, Fe, Mn and Mo elements from surface to center (b); EPMA map scanning results in the regions of surface (c1–c5), middle (defect band d1–d5) and center (e1–e5)

elements combined into the iron-rich phase and their distribution is almost the same [Figs. 4(c3, d3, e3) and Figs. 4(c4, d4, e4)]. The Mo element is almost distributed in the iron-rich phase while its content is lower compared with the Fe and Mn elements. Besides, iron-rich phase is mostly enriched in the defect band and center.

3.3 Morphology and distribution of ESCs and porosities

Figures 5(a) and (b) show the morphology and distribution of ESCs from surface to center under slow shot speeds of 0.1 m·s^{-1} and 0.4 m·s^{-1}, respectively. In the surface area, the ESCs are smaller in size due to a rapid cooling rate. However, in the defect band area, there is a lower distribution of ESCs, and the microstructure is mainly composed of eutectic structures. These larger ESCs tend to be located nearer to the center and exhibit a more pronounced dendritic morphology. Eventually, as approaching the center region, these ESCs develop into a network-like structure consisting of interconnected dendrites. When the slow shot speed is increased from 0.1 m·s^{-1} to 0.4 m·s^{-1}, there are noticeable changes in both the number and grain size of ESCs. Additionally, there is a reduction in the degree of dendritic morphology. The ESCs tend to exhibit a more spherical shape. Figure 5(c) shows the average diameter and the area fraction under slow shot speeds of 0.1 m·s^{-1} and 0.4 m·s^{-1}. With the increase of slow shot speed, the average diameter of ESCs decreases from 35.0 µm to 33.1 µm, and the area fraction decreases from 28.3% to 26.4%. Generally, the smaller average diameter and area fraction of ESCs are beneficial to the mechanical properties. Figure 5(d) shows the area fraction of ESCs from surface to center under slow shot speeds of 0.1 m·s^{-1} and 0.4 m·s^{-1}. The results indicate that under a slow shot speed of 0.1 m·s^{-1}, the area fraction of ESCs is distributed unevenly throughout the microstructure. The ESCs are mainly distributed in the position from 1,920 µm to 2,560 µm. Additionally, the content of ESCs is higher compared to a slow shot speed of 0.4 m·s^{-1}. With the increase of slow shot speed, the distribution of ESCs is more homogenized, indicating that higher slow shot speed can promote the homogenization of the microstructure. Figure 5(e) shows the average diameter from surface to center under different slow shot speeds. Under the slow shot speed of 0.1 m·s^{-1}, as approaching to the center, the average diameter of ESCs gradually increase, and the largest average diameter is about 47.0 µm. While, the largest average diameter of ESCs is about 35.6 µm under the slow shot speed of 0.4 m·s^{-1}. The increase in slow shot speed introduces disturbances to the flow

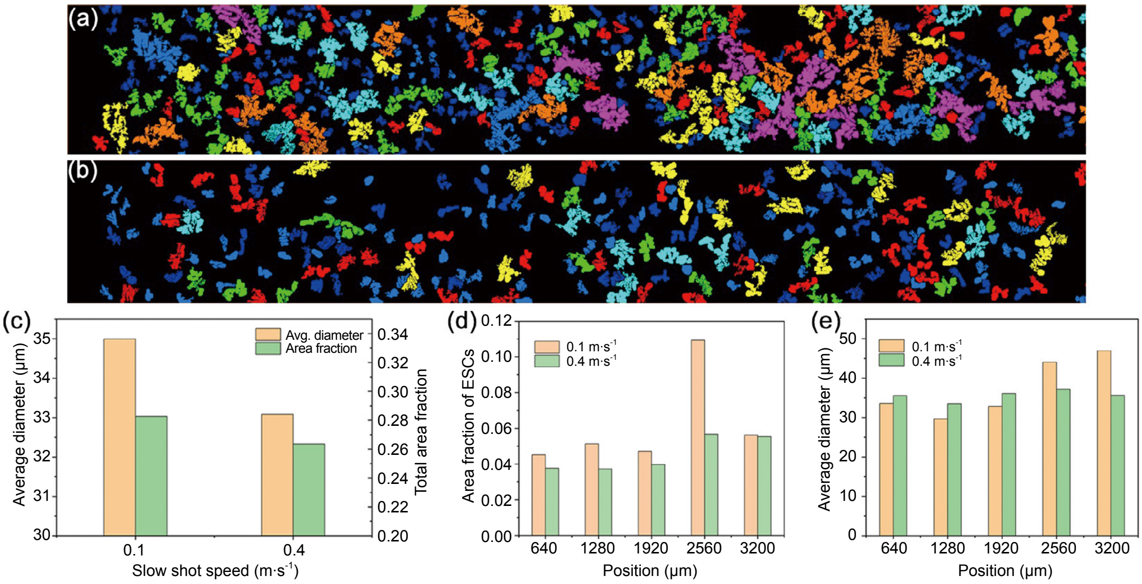

Fig. 5: Morphology and distribution of ESCs from surface to center under 0.1 m·s^{-1} (a) and 0.4 m·s^{-1} (b); average diameter and total area fraction vs. slow shot speed (c); area fraction (d) and average diameter (e) of ESCs from surface to center under different slow shot speeds

of metal during the casting process. These disturbances can have a scouring effect on ESCs. The high-speed flow can break or remelt larger ESCs, resulting in a reduction in their size. Furthermore, a higher slow shot speed decreases the residence time of metal flow within the shot sleeve. This reduced staying time limits the opportunity for large-size ESCs to form. With the increase of slow shot speed from 0.1 m·s^{-1} to 0.4 m·s^{-1}, both the number and the grain size of ESCs are reduced. Meanwhile, the distribution of ESCs is more dispersed in the casting samples, as shown in Figs. 5(a) and (b).

Figures 6(a) and (b) show the 3D porosity morphology of rod samples under slow shot speeds of 0.1 m·s^{-1} and 0.4 m·s^{-1}, respectively. When the slow shot speed is 0.1 m·s^{-1}, porosity has a strong clustering tendency in the center. Obviously, the number of porosities under the slow shot speed of 0.4 m·s^{-1} is fewer than that of 0.1 m·s^{-1}. Therefore, increasing slow shot speed is effective to reduce the number of porosities. Figures 6(a1) and (a2) indicate that the net shrinkage exhibits a large size. While, the porosities in Figs. 6(b1, b2) appear to be predominantly spherical with a smaller size. Figures 6(c) and (d) show the shape factor versus equivalent diameter of porosity under different slow shot speeds. Shape factor was used to measure the degree of regularity of porosities: 1 means the absolute sphere and 0 means the complete irregularity. The porosity with a larger equivalent diameter has a lower shape factor index, indicating a net shrinkage. With the increase of slow shot speed, the shape factor index tends to 1, indicating that the porosities gradually become round. Figure 6(e) shows the volume 3D and equivalent diameter under the slow shot speeds of 0.1 m·s^{-1} and 0.4 m·s^{-1}, respectively. When the slow shot speed is 0.1 m·s^{-1}, the porosities have a larger volume 3D and the maximum could be up to 1.7×10^4 mm^3. When the slow shot speed is 0.4 m·s^{-1}, the volume 3D reduces to 6×10^3 mm^3, and the equivalent diameter reduces from 26 μm to 22 μm. In addition, the volume 3D fraction of porosities reduces from 12.92% to 0.062% with the increase of slow shot speed. In general, with the slow shot speed increases, the number and volume fraction of porosities in the samples show a significant reduction, and the morphology is closer to be spherical.

The porosities in high-pressure die-cast Al alloy are generally resulted from the entrapped gas in chamber and solidification shrinkage. Higher slow shot speed can reduce the gas entrapped in the chamber. Furthermore, s slower slow shot speed can cause more temperature drop of Al melt in the chamber. Hence, after mold filling, the temperature of Al liquid in the die cavity is lower, which decreases the intensification pressure transmission from the plunger to the solidifying casting. A good pressure transmission can compress the entrapped gas pores during the initial stages of solidification and facilitate proper feeding to counteract shrinkage, resulting in a decrease in shrinkage porosity. As a result, the large gas pores with a high shape factor and the shrinkage porosities with a small shape factor are found in Figs. 6(c) and (d).

3.4 Mechanical property and fracture behavior under different slow shot speeds

Figure 7 shows the tensile properties under the slow shot speeds of 0.1 m·s^{-1} and 0.4 m·s^{-1} for rod samples of AlSi9MnMoV alloy. Significantly, with the increase of slow shot speed, the mechanical properties have a visible improvement, especially for elongation. The ultimate tensile strength is enhanced from 260.31 MPa to 290.31 MPa (increased by 11.52%), the elongation is enhanced from 3.72% to 6.34% (increased by 70.52%), and the yield strength slightly increased by 6.98%. This confirms that the reduction in size and number of ESCs and porosities can effectively enhance strength and plasticity.

Figures 8(a) and (b) show the crack surface of the rod samples under slow shot speeds of 0.1 m·s^{-1} and 0.4 m·s^{-1}, respectively. Obviously, the fracture under 0.1 m·s^{-1} strongly fluctuates and contains more gas pores. Lower slow shot speed

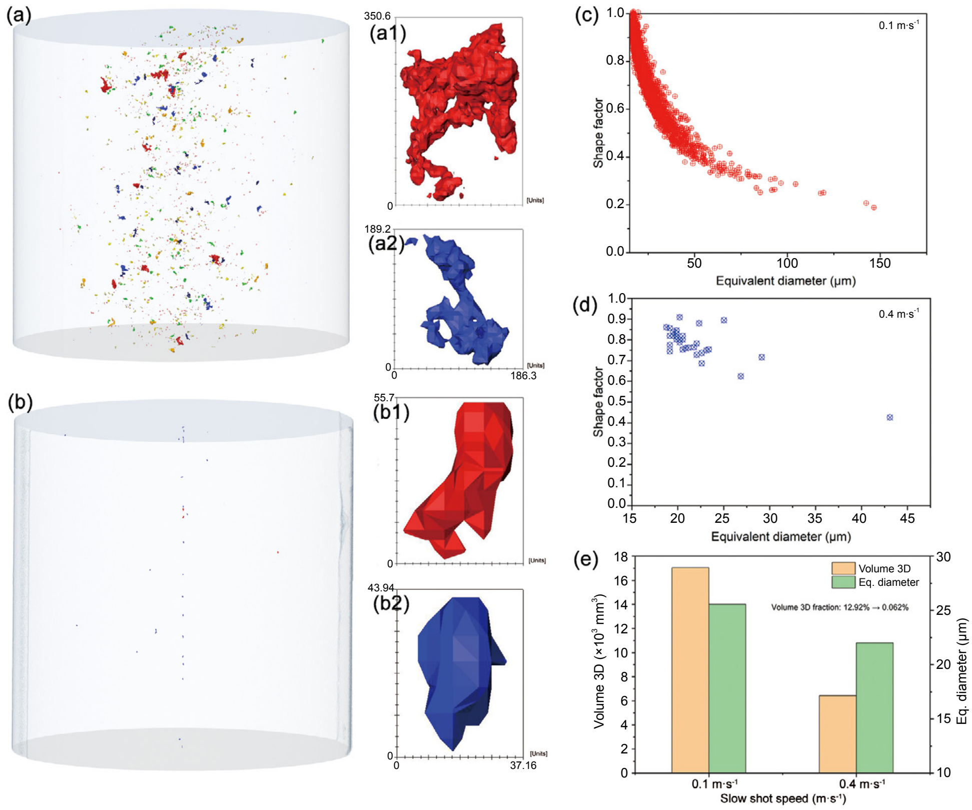

Fig. 6: 3D pore morphology under different slow shot speeds of 0.1 m·s^{-1} (a) and corresponding pores (a1) and (a2), and 0.4 m·s^{-1} (b) and corresponding pores (b1) and (b2); the shape factor vs equivalent diameter under slow shot speed of 0.1 m·s^{-1} (c), 0.4 m·s^{-1} (d); and the volume 3D and equivalent diameter under different slow shot speeds (e)

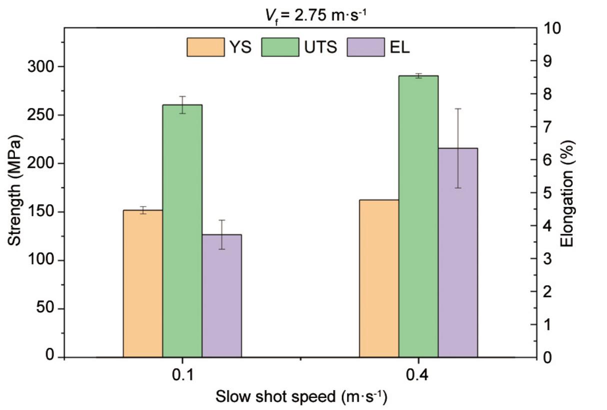

Fig. 7: Mechanical properties of AlSi9MnMoV alloy under different slow shot speeds

promotes the nucleation and growth of ESCs, causing the developed dendrite. The large ESCs are clustered together and form the dendrite net. At the final solidification, the ESCs contact with each other and the gaps couldn't be filled with metal liquid, which leads to the formation of shrinkage. Figures 8(c) and (f) show the pores under slow shot speeds of 0.1 m·s^{-1} and 0.4 m·s^{-1}, respectively. The results indicate that at a lower slow shot speed, the formation of large-size pores is more prevalent, leading to stress concentration. Consequently, cracks are more likely to initiate and propagate around these large-size pores under tensile forces, ultimately resulting in fracture. It can be seen from Fig. 8(d) that plenty of shrinkages are distributed on the fracture surface at slow shot speed of 0.1 m·s^{-1}, and form the net shrinkage. During the tensile process, the presence of stress concentration causes the stress levels at sharp corners of defects to be significantly higher compared to other areas. The maximum stress σ_{max} in the sample could be expressed by the following equation:

$$\sigma_{max} = \frac{KF}{A_0(1-f)} \tag{2}$$

where F is the tensile stress, K is the stress concentration factor related to the shape of the defect, A_0 is the cross-sectional area of the sample, and f is the percentage of the cross-sectional area occupied by the defect. When σ_{max} is greater than the fracture stress of the structure around the defect, the crack starts to propagate at the defect. Microcracks occur around the net shrinkage due to the stress concentration. These microcracks could expand and connect with each other under the tension and finally form a complete crack causing the failure of the rod samples.

Figures 8(e) and (h) show the ESCs morphology on the fracture surface under the slow shot speeds of 0.1 m·s^{-1} and 0.4 m·s^{-1}, respectively. The ESCs under the slow shot speed of 0.1 m·s^{-1} exhibit a larger size and the stress mainly concentrates around the boundary of ESCs, causing the intergranular fracture. According to the Hall-Petch equation:

$$\sigma_s = \sigma_0 + kD^{-\frac{1}{2}} \tag{3}$$

where σ_s is the yield strength of the material, σ_0 is the resistance of the material to deformation, k is an coefficient indicating the

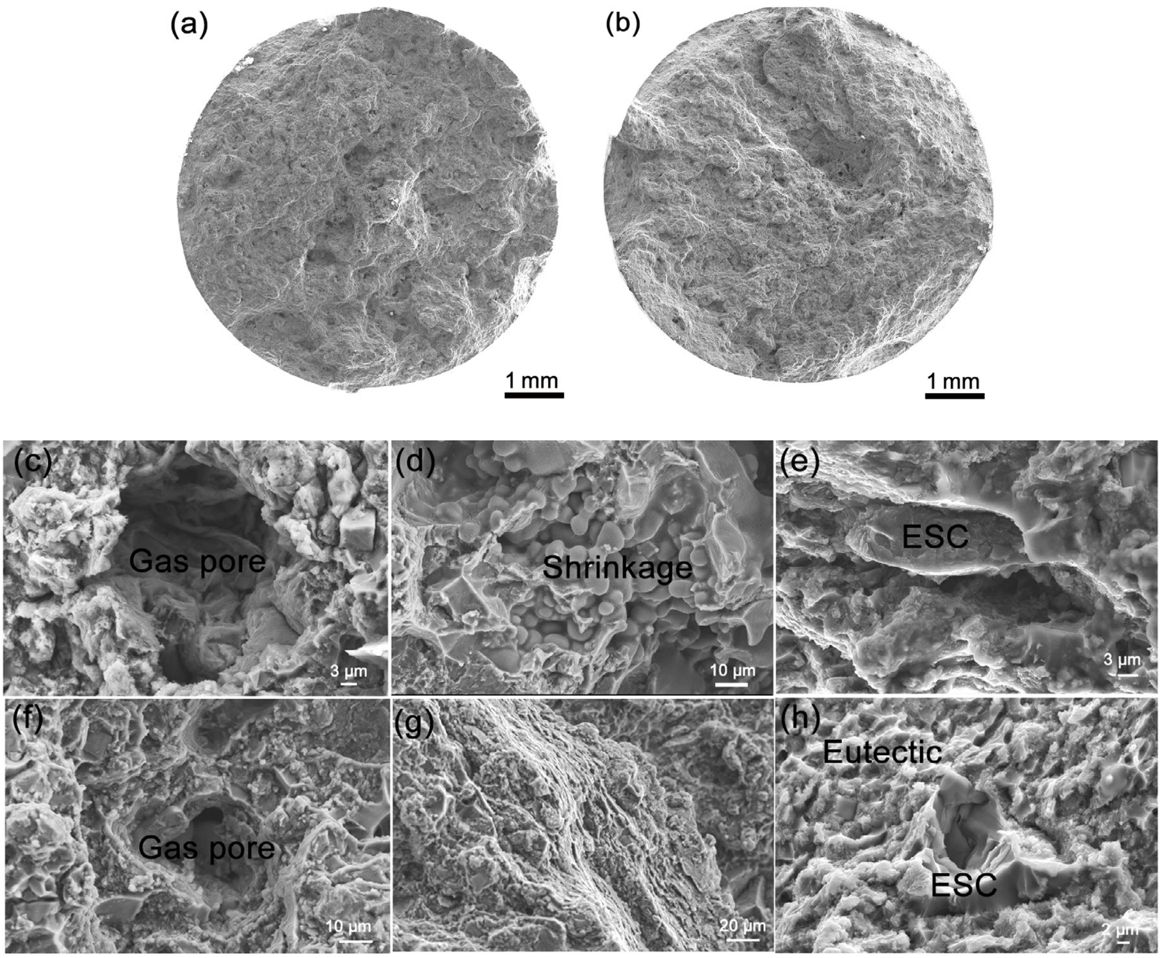

Fig. 8: Crack surface of rod samples at V_L=0.1 m·s^{-1} (a) and V_L=0.4 m·s^{-1} (b). (c, d, and e) indicate the fracture morphology of gas pore (c), shrinkage (d), and ESCs (e) at slow shot speed of 0.1 m·s^{-1}, and (f, g, and h) indicate the gas pore (f), shrinkage (g), ESCs (h) at slow shot speed of 0.4 m·s^{-1}

influence of the grain boundary structure on the deformation, and D is the average grain size. For alloys of defined composition, σ_0 and k are constants, so the average grain size variation of the grains determines the yield strength of the material. The smaller the average size value of the grains, the higher the yield strength.

Under the slow shot speed of 0.4 m·s^{-1}, the ESCs show a smaller size and are surrounded by the eutectics. Under tension, the eutectic Si phase is typically harder than ESCs and bears the majority of the applied force. This structure promotes coordination between ESCs and eutectic Si phase during deformation and results in enhanced mechanical properties. In conclusion, increasing the slow shot speed can lead to the realization of smaller gas pores, reduced shrinkage, and finer grain size of ESCs. Furthermore, adopting a higher slow shot speed significantly enhances the tensile properties.

4 Conclusions

(1) The microstructure of a newly developed AlSi9MnMoV alloy consists of coarse ESCs, fine $(\alpha\text{-Al})_{II}$, eutectic silicon phase and iron-rich phase. The AlSi9MnMoV alloy designed by trace multicomponent presents a significant refining effect compared with AlSi10MnMg alloy.

(2) A typical die casting heterogeneous microstructure is observed with the chilling fine grain in the skin layer, the silicon-rich zone in the defect band, and the ESCs-rich zone in the center.

(3) With the increase of slow shot speed, the size and quantity of ESCs and pores are significantly reduced, and the net-shrinkage disappears. Meanwhile, the distribution of ESCs is more dispersed in the casting samples.

(4) At lower slow shot speeds, it is easier for large ESCs to form and cluster together, eventually developing into a dendrite network. Within this dendritic boundary, larger ESCs have a higher tendency to form and cluster together, eventually creating a dendritic network. This stress concentration promotes crack propagation and ultimately increases the risk of casting failure.

Acknowledgments

This work was financially supported by the National Key Research and Development Program of China (2022YFB3404201), and the Major Science and Technology Project of Changchun City, Jilin Province (Grant No. 20210301024GX). The authors would also appreciate the help provided by China FAW Group Co., Ltd. and China FAW Foundry Co., Ltd. for the experimental cooperation.

Conflict of interest

The authors declare that they have no conflict of interest.

References

[1] Timelli G, Caliari D, Rakhmonov J. Influence of process parameters and Sr addition on the microstructure and casting defects of LPDC A356 alloy for engine blocks. Journal of Materials Science & Technology, 2016, 32: 515–523.

[2] Gjestland H, Westengen H. Advancements in high pressure die casting of magnesium. Advanced Engineering Materials, 2007, 9: 769–776.

[3] Weiler J P, Wood J T, Klassen R J, et al. Relationship between internal porosity and fracture strength of die-cast magnesium AM60B alloy. Materials Science & Engineering: A, 2009, 395: 315–322.

[4] Ye H. An Overview of the development of Al-Si alloy based material for engine applications. Journal of Materials Engineering and Performance, 2003, 12: 288–297.

[5] Cáceres C H, Selling B I. Casting defects and the tensile properties of an AlSiMg alloy. Materials Science and Engineering: A, 1996, 220: 109–116.

[6] Cavaliere P, Marco P. Fatigue behaviour of friction stir processed AZ91 magnesium alloy produced by high pressure die casting. Materials Characterization, 2007, 58: 226–232.

[7] Korti A I N, Abboudi S. Effects of shot sleeve filling on evolution of the free surface and solidification in the high-pressure die casting machine. International Journal of Metalcasting, 2017, 11: 223–239.

[8] Laukli H I, Gourlay C M, Dahle A K. Migration of crystals during the filling of semi-solid castings. Metallurgical and Materials Transactions A, 2005, 36: 805–818.

[9] Laukli H I, Arnberg L, Lohne O. Effects of grain refiner additions on the grain structures in HPDC A356 castings. International Journal of Cast Metals Research, 2005, 18: 65–72.

[10] Laukli H I. High pressure die casting of aluminium and magnesium alloys-grain structure and segregation characteristics. Ph.D. Thesis. Trondheim: Norwegian University of Science and Technology, 2004: 85–104.

[11] Dou K, Lordan E, Zhang Y J, et al. A complete computer aided engineering (CAE) modelling and optimization of high pressure die casting (HPDC) process. Journal of Manufacturing Processes, 2020, 60: 435–446.

[12] Wang Q L, Xiong S M. Vacuum assisted high-pressure die casting of AZ91D magnesium alloy at different slow shot speed. Transactions of Nonferrous Metals Society of China, 2014, 24: 3051–3059.

[13] Tsoukalas V D. The effect of die casting machine parameters on porosity of aluminium die castings. International Journal of Cast Metals Research, 2003, 15: 581–588.

[14] Fu P H, Luo A A, Jiang H Y, et al. Low-pressure die casting of magnesium alloy AM50: Response to process parameters. Journal of Materials Processing Technology, 2008, 205: 224–234.

[15] Cao H, Wessén M. Characteristics of microstructure and banded defects in die cast AM50 magnesium components. International Journal of Cast Metals Research, 2013, 18: 377–384.

[16] Jiao X Y, Wang J, Liu C F, et al. Influence of slow-shot speed on PSPs and porosity of AlSi17Cu2.5 alloy during high pressure die casting. Journal of Materials Processing Technology, 2019, 268: 63–69.

[17] Tzamtzis S, Zhang H, Babu N H, et al. Microstructural refinement of AZ91D die-cast alloy by intensive shearing. Materials Science & Engineering: A, 2010, 527: 2929–2934.

[18] Kim Y C, Choi S W, Kim C W, et al. Influence of process parameters on the fluidity of high pressure die-casting Al-Si alloys. Advanced Materials Research, 2013, 813: 171–174.

[19] Li X, Xiong S M, Guo Z. On the porosity induced by externally solidified crystals in high-pressure die-cast of AM60B alloy and its effect on crack initiation and propagation. Materials Science & Engineering: A, 2015, 633: 35–41.

[20] Jiao X Y, Zhang Y F, Wang J, et al. Characterization of externally solidified crystals in a high-pressure die-cast AlSi10MnMg alloy and their effect on porosities and mechanical properties. Journal of Materials Processing Technology, 2021, 298: 117299.

[21] Fan Z, Wang Y, Zhang Y, et al. Grain refining mechanism in the Al/Al-Ti-B system. Acta Materialia, 2015, 84: 292–304.

[22] Wang F, Qiu D, Liu Z, et al. The grain refinement mechanism of cast aluminium by zirconium. Acta Materialia, 2013, 61: 5636–5645.

[23] Zhao C, Li Y, Xu J, et al. Enhanced grain refinement of Al-Si alloys by novel Al-V-B refiners. Journal of Materials Science & Technology, 2021, 94: 104–112.

[24] Wang F, Qiu D, Liu Z, et al. Crystallographic study of grain refinement of Al by Nb addition. Journal of Applied Crystallography, 2014, 47: 770–779.

[25] Chen Z, Kang H, Fan G, et al. Grain refinement of hypoeutectic Al-Si alloys with B. Acta Materialia, 2016, 120: 168–178.

[26] Gourlay C M, Meylan B, Dahle A K. Shear mechanisms at 0–50% solid during equiaxed dendritic solidification of an AZ91 magnesium alloy. Acta Materialia, 2008, 56: 3403–3413.

[27] Gourlay C M, Dahle A K. Dilatant shear bands in solidifying metals. Nature, 2007, 445: 70–73.

[28] Hou Y, Wu M, Tian B, et al. Characteristics and formation mechanisms of defect bands in vacuum-assisted high-pressure die casting AE44 alloy. Transactions of Nonferrous Metals Society of China, 2022, 32: 1852–1865.